



## UvA-DARE (Digital Academic Repository)

### Mesosopic Computational Haemodynamics

Artoli, A.M.M.

**Publication date**  
2003

[Link to publication](#)

#### **Citation for published version (APA):**

Artoli, A. M. M. (2003). *Mesosopic Computational Haemodynamics*. [Thesis, fully internal, Universiteit van Amsterdam]. Ponsen en Looijen.

#### **General rights**

It is not permitted to download or to forward/distribute the text or part of it without the consent of the author(s) and/or copyright holder(s), other than for strictly personal, individual use, unless the work is under an open content license (like Creative Commons).

#### **Disclaimer/Complaints regulations**

If you believe that digital publication of certain material infringes any of your rights or (privacy) interests, please let the Library know, stating your reasons. In case of a legitimate complaint, the Library will make the material inaccessible and/or remove it from the website. Please Ask the Library: <https://uba.uva.nl/en/contact>, or a letter to: Library of the University of Amsterdam, Secretariat, P.O. Box 19185, 1000 GD Amsterdam, The Netherlands. You will be contacted as soon as possible.

# Chapter 8

## The Real Thing

Based on the arguments raised on the previous chapters, in this chapter, simulation results of steady and unsteady flow in a realistic model of the human aortic bifurcation reconstructed from Magnetic Resonance Angiography are presented as a typical haemodynamic application. Velocity fields and shear stress are computed and results are compared to those available in the literature.

### 8.1 Introduction

Flow characteristics near branches and bifurcations are quite important in haemodynamics: Cardiovascular diseases are considered as a leading cause of death in the developed world and are now becoming more prevalent in developing countries (World Health Organisation, 2002). Most of these diseases localise in regions of complex geometry of the arterial tree. The flow fields and shear stress play important roles in understanding, diagnosis and treatment of such diseases. Although being studied by many authors (e.g. McDonald, 1960; Caro *et al.*, 1974; Ku *et al.*, 1985; Moore *et al.*, 1994a, 1994b and 1994c; Reneman *et al.*, 1993; Taylor *et al.*, 1996; Gijzen *et al.*, 1997; Vorp *et al.*, 1998; Wootton, 1999; Ku, 1999), the relation between flow fields and cardiovascular diseases is still not fully understood, and is currently receiving more and more attention (Botnar *et al.*, 2000, Berthier *et al.*, 2002; Cheng *et al.*, 2002).

There have been many reports relating low and oscillatory shear stress to atherosclerosis in large arteries. For a recent review, we refer to Shaaban and Duerinckx (2000). Frequently, the treatment of an arterial disease involves implanting a new host artery as an additional or a replacement to the diseased one, or design of a cardiovascular device. These are quite difficult to plan and have to be tailor made for each specific patient.

Recently, two major developments in the field of vascular surgery planning have made it possible to better and faster plan risk reduced implantation: firstly, magnetic resonance imaging angiography (MRA)<sup>1</sup> has been significantly enhanced to provide ex-

---

<sup>1</sup>use of Magnetic Resonance Imaging to produce detailed pictures of the blood vessels.

cellent images of the arterial tree and non-invasive dynamic data acquisition is made possible (Goyen *et al.*, 2001). Secondly, the development of cheap computing power and interactive simulation environments have made near real time simulations not far from reach (Taylor *et al.*, 1999; Bellemann and Sloot, 2000; Zao *et al.*, 2002). With these in hand, an efficient and robust flow solver can be used as an interactive modelling environment. There are various successful computational fluid dynamics (CFD) methods commonly used here, such as the finite element methods, the finite difference methods and the finite volume methods. All these techniques are well established, but they yield two major difficulties. These are the non-trivial and time consuming grid generation, and the necessity to solve the Poisson equation for the pressure field.

On the other hand, the conventional flow solvers such as the finite element methods and the finite difference methods are accurate and efficient. However, their applicability to problems involving complex and moving geometry is complicated, due to their strong dependence on time consuming mesh generation. The Navier-Stokes (NS) equations can now be solved with mesh-free algorithms (Batina, 1993) which are unfortunately not flexible enough due to errors attributed to numerical viscosity and to difficulty in improving the space and time accuracy. Dynamic mesh generating techniques have been reported recently (Taylor *et al.*, 1998).

New particle based methods such as dissipative particle dynamics, lattice gases and lattice Boltzmann methods have been developed and matured (Mcnamara and Zanetti, 1988; Higuera and Succi, 1989; Qian *et al.*, 1992; Aharonov and Rothman, 1993; Behrend, 1995). These mesoscopic techniques may be quite useful for haemodynamic research, as, among other features, they are more flexible in dealing with multicomponent fluid flow problems. In this study, we use the lattice Boltzmann BGK method, shortly described in the next section.

Since the shear rate in the aorta is higher than  $0.1s^{-1}$ , we consider blood to be Newtonian. We also ignore the elastic behaviour of the aortic walls for its minor effects on the flow fields in the aorta.

As time dependent flow simulations are known to be computationally expensive, a need for an efficient flow solver is crucial. Traditional Navier-Stokes solvers frequently use artificial compressibility and pressure projection methods to accelerate convergence. In this study, we present the capability of the lattice Boltzmann BGK method as a robust technique for systolic Newtonian flow in a complex model of the human abdominal aorta reconstructed from MRA images of a volunteer.

Different from the traditional CFD methods which obtain the velocity and pressure by solving the Navier-Stokes equations and compute the shear stress from the velocity profiles, the lattice Boltzmann BGK method is a special finite difference equation of the simplified Boltzmann BGK equation which describes transport phenomena at the mesoscopic level. From the previous chapters, it has been realised that solving the lattice Boltzmann equation has three main advantages over solving the Navier-Stokes equations: first, it works with fast and easy to generate Cartesian grids while it still yields accurate results of second order in space and time. Secondly, the pressure is simply a linear function in the speed of sound ( $p = \rho c_s^2$ ) while the NS solvers need to

solve the Poisson equation. Finally and most important for the field of haemodynamics, is the fact that the stress tensor can be directly obtained from the non-equilibrium parts of the distribution functions, independent of the velocity fields, while a need to get the derivative of obtained velocity profiles is not avoidable when NS solvers are used. The non equilibrium parts of the distribution functions are computed during collision steps to relax the system towards equilibrium. Therefore, no considerable computational cost is needed to compute the stress. All these advantages make the lattice Boltzmann method a promising candidate for simulating time-dependent blood flow in arteries.

In the last two chapters, it has been demonstrated that the lattice Boltzmann method can easily be adapted to simulate time dependent flows. Since it is a linear function in the pressure, time dependent density gradients can be implemented to represent a systolic flow rate quite easily. A range of values of Womersley parameter can be simulated without affecting the stability of the model. All kinds of inlet and outlet boundary conditions, usually used in computational haemodynamics can equivalently be implemented. The robustness of the method appears in the straightforward parallelisation of the easy to generate Cartesian grid. On the other hand, since it is implemented on a Cartesian grid, very fine grids need to be generated to simulate flow in complex geometry. Filippova and Hänel (1998) have overcome this problem by considering local grid refinement.

## 8.2 Flow in the Abdominal Aorta

Atherosclerosis mainly occurs in focused locations of large and medium arteries such as the carotid bifurcation, the coronary arteries, the abdominal aorta and the iliac and femoral arteries at regions of low and oscillating shear stress, independent of other risk factors (Shaaban and Duerinckx, 2000). In the human abdominal aorta, the lateral and posterior walls of the aorta distal to the inferior mesenteric artery (IMA) are highly susceptible for Atherosclerosis. These regions are known to have low and oscillating shear stress (Gibson *et al.*, 1993; Oshinski *et al.*, 1995; Taylor *et al.*, 1998). From the arguments raised previously and the conducted benchmark experiments presented earlier in this thesis, we are further encouraged to explore the capability of the lattice Boltzmann method in simulating a more realistic geometry of interest to Biomechanics. We choose to study flow in a model of the human abdominal aorta as an example. The model is reconstructed from a magnetic resonance angiography of a volunteer. The pressure gradient at the entrance of the aorta is averaged from flow rate obtained from literature (Moore *et al.*, 1994c; Taylor *et al.*, 1999). The computational model under study involves only the bifurcation region, directly after the IMA, and includes parts of the left and right iliac arteries (see Fig. 8.1). The complete model of the abdominal aorta, including the celiac, mesenteric and renal branches is currently under study.

Many studies on the flow in the abdominal aorta have been reported, all related the cause of the focal nature of the disease mainly to the complex nature of the shear

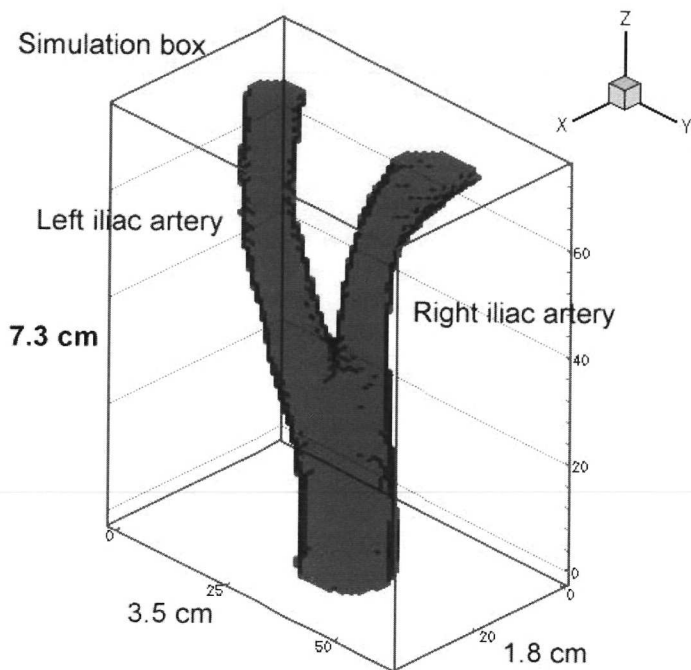


Figure 8.1: An MRA reconstructed model of the aortic bifurcation with left and right iliacs. The right iliac is more bent than the left one. The computational grid size is  $37 \times 61 \times 73$  nodes.

stress profiles in these regions. Several investigations have been discussed in literature. Moore *et al.* (1994a) computed the shear stress in a model of the human abdominal aorta under resting and exercise conditions from MRA measured velocity data and extracted six shear stress indices influencing the locality of Atherosclerosis: mean (over the cardiac cycle), maximum and minimum, pulse (maximum - minimum), negative index, NEG (fractional time during which the shear stress stays negative) and oscillatory shear stress index (OSI). Reneman *et al.* (1993) used experimental and computational models to study flow in bifurcation regions. Gijssen *et al.* (1997) suggested a new experimental technique to determine the wall shear stress *in vivo*. Vorp *et al.* (1998) used a coupled fluid structure interaction model to combine the influence of mechanical stress and wall shear stress and concluded that the arterial diseases most probably localise in regions of high mechanical stress and low wall shear stress. However, the mechanical stress within the wall cannot easily be extracted unless further development in imaging techniques and image segmentation algorithms are achieved. In this study, we use Eq.(3.22) to compute the 9 components of the sym-

metric stress tensor, i.e.  $\sigma_{\alpha\beta}$  which represents the stress component in the  $\beta$ -direction acting on the element with outward normal in the  $\alpha$ -direction. Since the components of any second order tensor can be reduced to an eigenvalue problem, it is possible to transform the second order stress tensor into an eigenvalue problem and extract the principal stresses  $\lambda_1$ ,  $\lambda_2$  and  $\lambda_3$  with their eigen vectors. These can be visualised as a quadric surface (elliptical glyph), but in biomechanics, the traction forces, shear stress and the von Mises effective stress are commonly used. The traction forces are orientation dependent and need the surface normals. However, the von Mises effective stress, usually available in visualisation packages, is computed from the second invariant of the stress tensor (see the next section) and is more suitable for Cartesian grids than the surface traction, as the Cartesian grids introduce more approximation when computing surface normals. The von Mises stress is commonly used in biomechanics to determine the effective stress (e.g.. Raghavan and Vorp, 2000). In this study, we will focus on the time-behaviour of the effective von Mises stress.

For our simulations, a smoothed MRA image was provided by Charles Taylor, Stanford University, U.S.A, with original resolution of  $512 \times 512 \times 64$  voxels, each voxel occupies 1 byte. The spacing between each two successive recorded cut planes is 0.9375 mm. An image segmentation algorithm is applied to the original data set to extract the aorta and the segmented aorta is then cropped and filtered to end up with the simulation model shown in Fig. 8.1. It is worth noting that there is a limitation

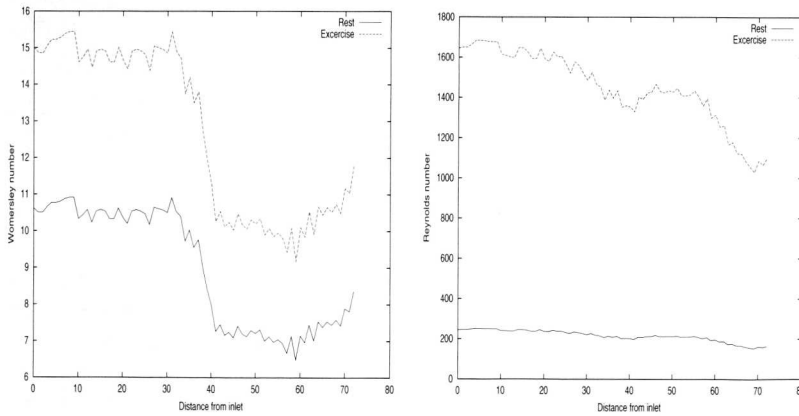


Figure 8.2: Change in Womersley parameter(left) and Reynolds number (right) along the segmented aorta during resting and exercise conditions.

to obtaining high resolution non-invasive and low noise images. To have a stable solution in the lattice Boltzmann method, the relaxation time  $\tau$  must be greater than 0.5 in order to have a positive fluid viscosity. Having a Reynolds number  $R_e$  within a diameter  $nD$ ,  $n$  being the spatial resolution of the image, for a fluid of blood viscosity, will result in a relaxation time of  $0.5 + 0.3nD/R_e$ . Therefore, the stability scales linearly with the spatial resolution. We have conducted a number of steady and

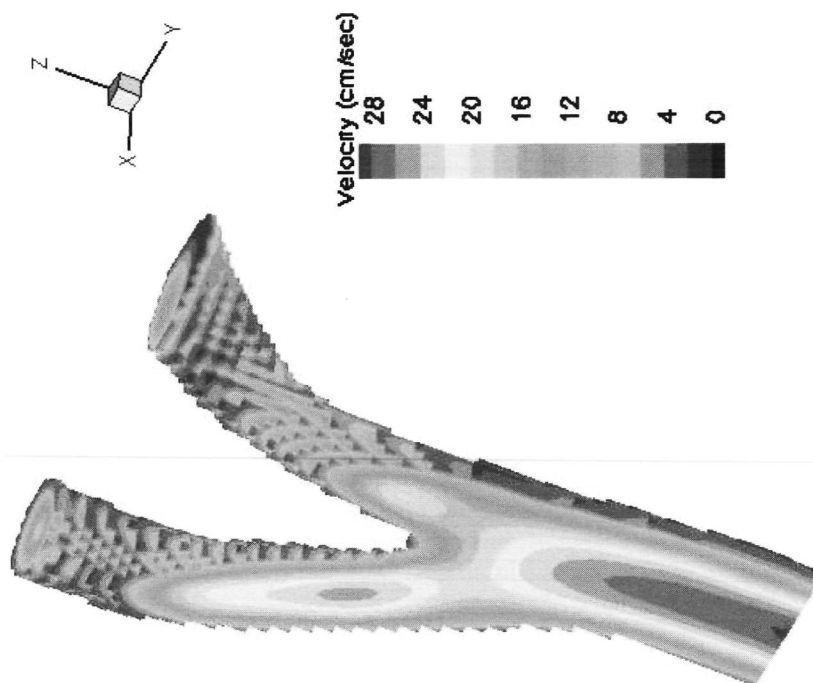


Figure 8.3: Steady flow in the aortic bifurcation. The maximum Reynolds number is 1500.

unsteady flow simulations for the aorta model. As the cross section of each slice is irregular, the Reynolds number is redefined as  $Re = 4mU/v = \frac{4Q}{vP}$  and the Womersley number is defined as  $\alpha = 2m\sqrt{\omega/v}$ , where  $m$  is the mean hydraulic depth which is the ratio between the vascular bed  $A$  and the perimeter  $P$ . Figure 8.2 shows changes in the Reynolds and the Womersley numbers downstream of the aortic model under resting and exercise conditions, assuming a flow rate of 0.8 l/min with 65 beats/min under resting and 5.36 l/min with 130 beats/min for exercise conditions (Moore and Ku, 1994d).

The steady flow simulations are performed to assess the steady flow behaviour and to check the validity of the used inlet and outlet conditions. We have used the bounce-

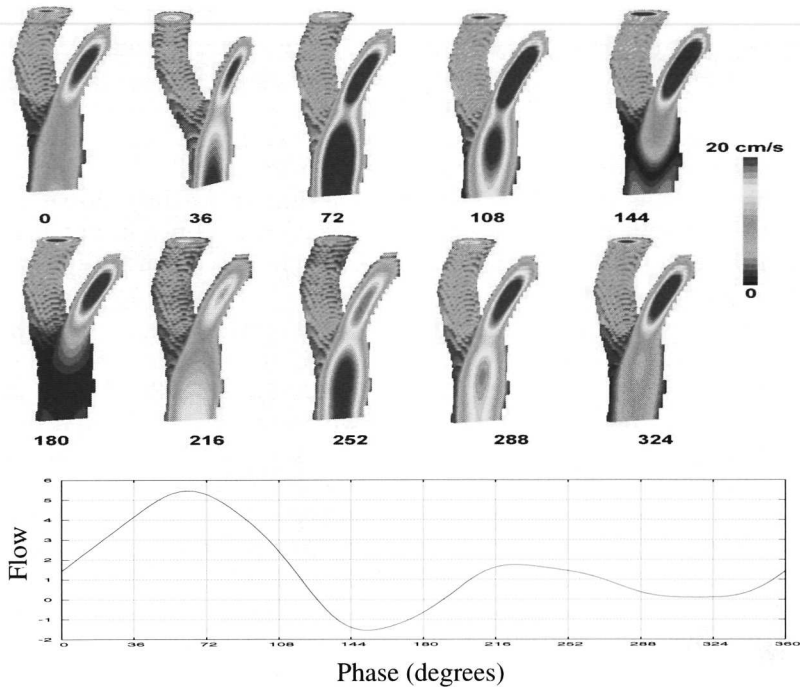


Figure 8.4: Velocity profiles in the aortic bifurcation computed at every  $36^\circ$  of the cardiac cycle, at 120 heart beats/min and a flow rate of  $90 \text{ cm}^3/\text{sec}$

back rule as a wall boundary condition. For the inlet, we use an assigned inlet pressure to compute the inlet velocity (Zou and He, 1997) and assign equilibrium values for unknown distributions. The outlet conditions are assigned accordingly with an outlet pressure. The maximum Reynolds number is 1500. A velocity snapshot of steady flow is shown in Fig. 8.3, from which we observe that the bended branch of the aorta (the right iliac in this case) has less entrance velocity than the less curved one (the left iliac). The velocity gradients before the bifurcation are smaller near to the right lateral wall than those on the left lateral wall and the shear stress is expected to be smaller. Also, the posterior wall receives less flow than the anterior wall and a similar conclusion may be drawn. However, the unsteady nature of the locality of low shear stress may be different as will be explained later.

For the unsteady flow simulations, an aortic pressure waveform is applied at the entrance of the aortic model. Velocities are then computed from the distribution functions coming from downstream, and the unknown distributions are set to their equilibriums. At the two outlets, constant pressure is applied. The total simulation time is 2 hours on a single processor and reduces to 40 minutes when using 4 nodes. We assume that the system converges after the change in conserved quantities (mass and

momentum) is less than  $2 \times 10^{-5}\%$ . This results in an error that is less than 1% when simulating rigid circular tubes, as claimed in the previous section. At least 40 complete periods are needed to converge to the simulation criterion. Although it seems longer than the required periods when using a finite element solver, the total simulation time per period is far less. On a single processor, a period represented by 240 time-steps takes approximately 3 minutes. Flow fields and shear stress are recorded during the last cycle as separate frames for each time-step. The phase of the full cardiac cycle ( $360^\circ$ ) is split into a number of frames (vertical lines in Fig. 8.4) and each frame is named after the corresponding phase angle. Vector magnitudes of velocity profiles at 10 frames are visualised in Fig. 8.4.

At the beginning of systole (frame 0), the flow is relatively simple through the bifurcation model, except for a small velocity of maximum magnitude 5.0 cm/sec near to the walls of the main branch. As the flow is increased (frames 36 and 72), the velocity increases rapidly in the main branch and slowly in the iliacs. The left iliac receives more flow than the right one (see the change in the red dot on top of the branch). Close to the Aortic bifurcation, negative velocities of small magnitudes are frequently observed (see Fig. 8.5). The flow then relaxes towards the end of systole (frame 108). After that, a complex nature of the flow takes place in the main branch (see frames 144 and 180), involving two conjugate vortexes and flow mixing. This is clearly illustrated by streamlines shown in Fig. 8.6. It is worth noting that, although the flow reverses in the main branch during this period, the flow at the exits is forward on average. This demonstrates the function of the aorta as a reservoir that provides blood to the organs when the flow reverses. The second half of the cycle represents the diastole (frames 216-324) during which the flow oscillates till it reaches the beginning of systole where frame 0 is repeated.

Velocity magnitudes near the posterior wall are approximately the same as those close to the anterior wall, as shown by the symmetry in colour. Throughout most of the cardiac cycle, the flow is slightly skewed towards the anterior wall (Fig. 8.4).

Close to the bifurcation, the flow becomes quite complex. At about 15 mm proximal to the bifurcation, the flow reverses near the walls during most of the cardiac cycle. It was reported that the walls proximal to the aorta are frequently subjected to occlusive atherosclerosis, although this region does not involve bifurcation or area expansion which are two major factors that complicate the flow pattern (Moore *et al.*, 1994c). The locality of atherosclerosis in this straight segment is attributed to the low and oscillatory near wall velocity profiles, which may result in mass transfer from blood to the walls (Moore *et al.*, 1994c; Taylor *et al.*, 1996).

After the bifurcation, the flow is laminar. The left iliac receive more flow during systole. In order to have a clearer picture about the flow, streamlines are plotted for the whole cardiac cycle. Except for periods of back flow, the streamlines are in general uniform and show forward direction of the flow (data not shown). Vortex rings set up during flow reversal at the end of systole (See Fig. 8.6), but they progressively damp out when the flow is re-established. These vortices form a trap for fluid elements and disturb the flow across the whole vessel. The reason for formation of vortices may be attributed to the rapid flow reversal and the damp-out may be forced by the inher-

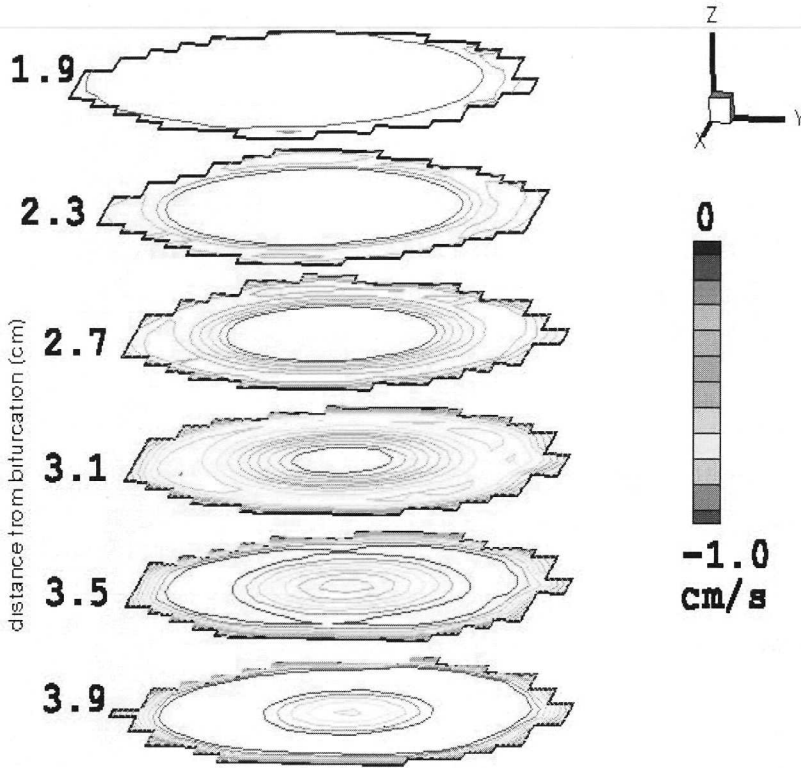


Figure 8.5: Negative velocity profiles during the systole are frequently observed close to the aortic bifurcation. The figure shows two snapshots of velocity 2.0 cm proximal to the bifurcation.

ent stability of the flow. Some of these observations have been previously reported by Moore *et al.* (1994c) in their extensive experimental MRA velocity measurements of a glass blown idealised model of the abdominal aorta and by Taylor *et al.* (1996) who observed large vortex development along the wall of the abdominal aorta, which shrinks considerably under moderate exercise condition. It is worth noting that although the models investigated by Moore *et al.* (1994c) and by Taylor *et al.* (1996) are idealised, similar qualitative results could be observed.

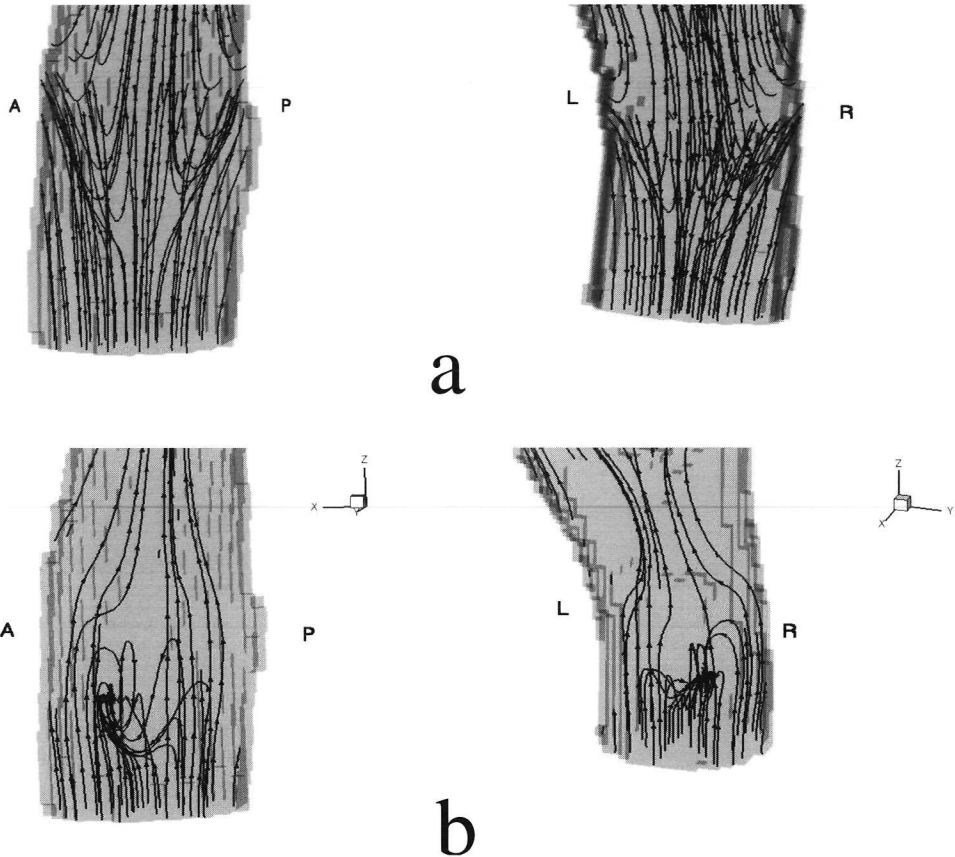


Figure 8.6: Velocity streamlines showing (a): Vortex formation during diastole (at  $t = 0.4T$ ) and (b) flow mixing (at  $t = 0.5T$ ).

### 8.3 Shear Stress

Shear stress for a Newtonian fluid is conventionally estimated from gradients of measured or simulated velocity components, and the fluid viscosity. This process involves some approximations which may lead to underestimation on the order of 10%–45% (Luo *et al.*, 1993) when the lumen is not circular. This large error is due to nonlinear velocity profile at the wall and ignorance of the radial derivatives. An enhancement was recently reported by Cheng *et al.* (2002) by introducing piecewise Lagrangian basis functions and segmenting the vessel lumen with a level set method.

With LBM, the nine Cartesian components of the local stress tensor are directly obtained using Eq. (3.22), as stated above without any further approximation than the Cartesian geometry. The stress at any given point is completely determined by this

stress tensor. A real benefit of the lattice Boltzmann solver is that these components are computed independently from velocity gradients. In this study, we compute and visualise the von Mises effective stress (Geiringer, 1953), defined as

$$\sigma_{eff} = \sqrt{\frac{A + 6B}{2}} \quad (8.1)$$

where

$$A = (\sigma_{xx} - \sigma_{yy})^2 + (\sigma_{yy} - \sigma_{zz})^2 + (\sigma_{zz} - \sigma_{xx})^2 \quad (8.2)$$

and

$$B = \sigma_{xy}^2 + \sigma_{yz}^2 + \sigma_{zx}^2. \quad (8.3)$$

This quantity is one of the three invariants of the stress tensor and therefore, is orientation independent. In addition, it includes the effect of small directional variations in the octahedral normal stress (the mean pressure) on the walls. The quantity  $B$  vanishes in the principal coordinate system.

The effective stress in  $\text{dynes/cm}^2$  is shown in Fig. 8.7, from which we observe that the effective stress at the posterior and lateral walls is always small (less than  $40 \text{ dynes/cm}^2$ ) throughout the cardiac cycle. The stress is uniformly distributed along the lateral walls. The minimum stress values are observed during the flow reversal where the stress is very small through the whole vessel. The stress also oscillates in magnitude and the stress vector oscillates rapidly. The high stress values near the exits of the left iliac are attributed to the fact that this branch is subject to a small curvature at these locations. Effects of outlet conditions are minor and are hardly seen. The stress behaviour during the systole is described below. Let us first describe the stress behaviour in the main branch. At the beginning of systole (frame 0), the shear stress is small (less than  $20 \text{ dynes/cm}^2$ ) and is least around the walls, with the posterior and right lateral walls having minimum values close to zero. The lateral walls of the left iliac have higher shear stress than the lateral walls for the right iliac, as predicted by the steady flow simulations.

The shear stress increases close to the walls as the systolic pressure is increased (frame 36) a strip-like island of zero shear stress splits the region just before the bifurcation into a left and right regions, with the left region having higher stress than the right one. The left anterior walls receive more stress (frame 72) of magnitude greater than  $60 \text{ dynes/cm}^2$ . Then the walls around the main are released from regions of minimum stress (frame 108), with the posterior walls released first while the anterior walls are not (frame 144). When the systole ends and the diastole begins (frame 180), the shear stress becomes again very small at regions far from the bifurcation, with small islands in the centre with minimum shear stress. The stress on the anterior lateral walls then increases, except for a small island in the middle of posterior wall, just before the bifurcation (frame 216). The shear stress comes again to its minimum on the centres and at the distal posterior walls (frame 252), with maximum shear stress ( $40 \text{ dynes/cm}^2$ ) on the walls. Then it gets smaller again, except near the left anterior walls (frame 288). Near the end of the cardiac cycle (frame 324), the

shear stress is low around the walls and on islands close to the bifurcation, spreading from left posterior to right anterior and covering the right anterior sides. The left anterior walls clearly has larger shear stress than the right side. At the end of the cycle, frame 0 is repeated.

In summary, the posterior wall receives stresses greater than 60  $\text{dynes/cm}^2$  during one third of the cycle, less than 5  $\text{dynes/cm}^2$  during another third and between 20 – 40  $\text{dynes/cm}^2$  during the rest of the cycle. The shear stress after the bifurcation is higher in magnitude than the main branch, except for some islands and edges.

At the beginning of systole (frame 0), the regions directly after the bifurcation have minimum shear stress in an island on the right iliac spreading toward the right lateral and posterior walls, while the left iliac has higher magnitudes on the outer walls and minimum values on the inner walls. The bend near the exit makes the shear stress highest at these locations ( $> 150 \text{ dynes/cm}^2$ ). The stress is also maximum in the centre of the exit of left iliac artery and one-third from the exit of the right iliac. The inner walls of the right iliac receive minimum shear stress. The near-end (after the bend) outer walls receive minimum shear stress. In summary, at the beginning of systole, the inner walls have less stress than the outer ones and the right iliac artery has less shear stress than the left one.

As the systole develops, the stress first goes higher towards the bifurcation (frame 36), but remains minimum for some islands on the right iliac: close to the bifurcation and near the inner posterior walls (frame 72). Near the exits, the stress at the anterior walls of the left iliac becomes minimum at the bend (frame 108), and gets less for the inner walls. The islands in the right iliac are shifted towards the posterior inner walls (frames 144 and 180) till they are accompanied by high stress islands spreading toward the outer and anterior walls of both iliacs (frame 216). The stress reaches its maximum directly after the beginning of diastole (frame 252) and oscillates around lesser values (frames 288 and 324) till the systole begins again (frame 0).

From this description, we see that the effective von Mises stress is minimum close to the lateral and posterior walls of the abdominal aorta segment before the bifurcation, at the inner walls of the iliacs, and at islands in the right iliac artery; and is maximum at anterior walls, outer walls of the iliacs and at islands on both iliacs. Comparable results have been obtained in the literature (e.g. Raghavan and Vorp, 2000; Moore *et al.*, 1994b; Taylor *et al.*, 1996) leading to similar conclusions about the relationship between locality of cardiovascular diseases and the complex nature of stress. However, in this study, we did not measure the oscillatory shear index, although it is known to have an influence on the locality of cardiovascular diseases. This will be presented in a future article in which the full abdominal aorta will be studied.

## 8.4 Summary

We have demonstrated that the lattice Boltzmann method is a successful mesoscopic solver to time dependent blood flow in the arterial system. Simulated results of sys-

tolic flow in a 3D rigid tube at haemodynamic Reynolds and Womersley parameters have recovered the analytic Womersley solutions within acceptable accuracy. Steady and unsteady flow fields in a realistic aorta geometry, reconstructed from Magnetic Resonance Angiography have been successfully obtained and compared to the available literature, showing qualitative agreements. As the shear stress plays a crucial role in cardiovascular diseases and since it is directly and independently computed in the lattice Boltzmann solver, we strongly encourage researchers from haemodynamics to consider this method as an alternative blood flow solver. More benefits are seen from easy grid generation and straightforward parallelism, easy and feasible adaptation to changing geometry. Further investigation of the complete aorta model and experimental validations are under development in our group.

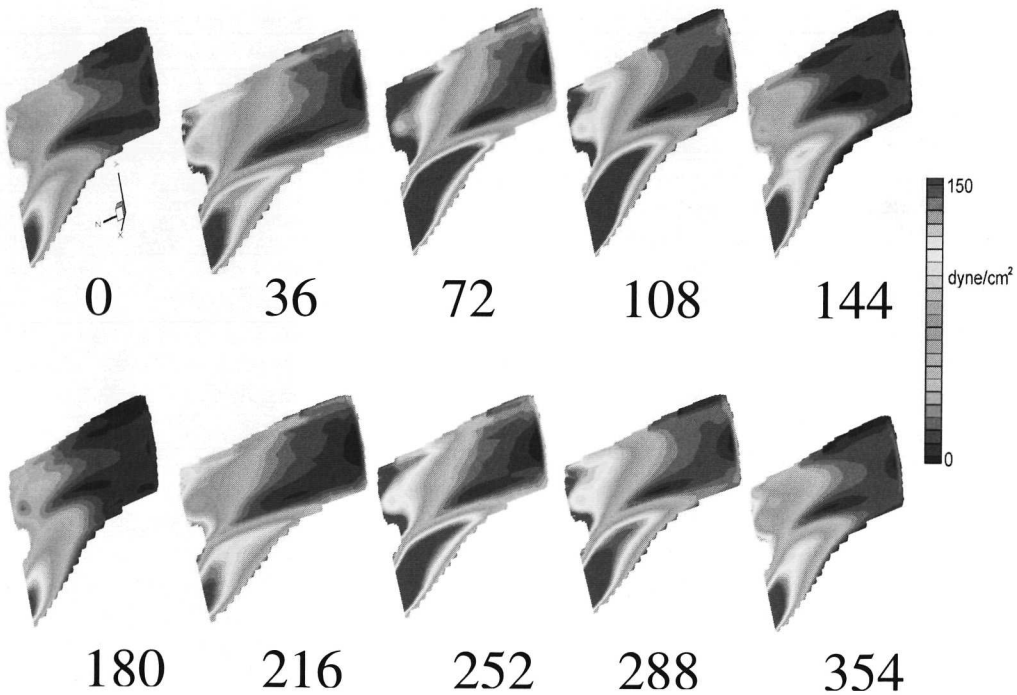


Figure 8.7: Effective stress on the walls of the aortic bifurcation computed at every  $36^\circ$  of the cardiac cycle. The posterior wall has low values throughout the whole systolic cycle, while relatively high values of the stress near the curved exits are observed.

